

# The deterioration of Circular Mausoleum, Roman Necropolis of Carmona, Spain

Juan C. Cañaveras<sup>a</sup>, Angel Fernandez-Cortes<sup>b,c</sup>, Javier Elez<sup>d</sup>, Soledad Cuezva<sup>b,c</sup>, Valme Jurado<sup>e</sup>, Ana Zelia Miller<sup>e</sup>, Miguel A. Rogerio-Candelera<sup>e</sup>, David Benavente<sup>a</sup>, Mariona Hernandez-Marine<sup>f</sup>, Cesareo Saiz-Jimenez<sup>e,\*</sup>, Sergio Sanchez-Moral<sup>b</sup>

<sup>a</sup>Departamento de Ciencias de la Tierra y del Medio Ambiente, Universidad de Alicante, 03080 Alicante, Spain

<sup>b</sup>Museo Nacional de Ciencias Naturales, MNCN-CSIC, Jose Gutierrez Abascal 2, 28006 Madrid, Spain

<sup>c</sup>Geomnia Natural Resources SLNE, 28003 Madrid, Spain

<sup>d</sup>Departamento de Paleontología, Universidad Complutense, 28040 Madrid, Spain

<sup>e</sup>Instituto de Recursos Naturales y Agrobiología, IRNAS-CSIC, Avenida Reina Mercedes 10, 41012 Sevilla, Spain

<sup>f</sup>Facultad de Farmacia, Universidad de Barcelona, 08028 Barcelona, Spain

## ABSTRACT

The Circular Mausoleum in the Roman Necropolis of Carmona was carved on a calcarenite sequence in an ancient quarry located in the town of Carmona, Southern Spain. This rock-cut tomb, representative of Roman burial practices, currently suffers from serious deterioration. A detailed survey over several years permitted the identification of the main tomb's pathologies and damaging processes, which include loss of material (scaling, flaking, granular disintegration), surface modifications (efflorescences, crusts and deposits) and extensive biological colonization. The results obtained in this study indicated that anthropogenic changes were largely responsible and enhanced the main alteration mechanisms observed in the Circular Mausoleum. Based on the deterioration diagnosis, effective corrective actions were proposed. This study shows that any conservation intervention in the interior of the tomb should be preceded by accurate *in situ* measurements and laboratory analyses to ascribe the source of the deterioration damages and thus designing effective treatments.

\*Corresponding author at: Instituto de Recursos Naturales y Agrobiología, IRNAS-CSIC, Avenida Reina Mercedes 10, 41012 Sevilla, Spain

*E-mail address:* saiz@irnase.csic.es

## 1. Introduction

The first tomb of a Roman Necropolis in the area of Carmona (province of Seville, Spain) was accidentally discovered in 1830 (Rada y Delgado, 1885; Maier Allende, 1999) although a few more tombs were exhumed between 1868 and 1869. These tombs were plundered until the archaeological excavations started in 1882. This necropolis, located in the town of Carmona represents one of the most significant Roman burial sites in Southern Spain, and was in use during the 1st and 2nd centuries AD. Initially, the necropolis was used as quarry from which stone blocks were extracted and used for building construction. The quarry was then abandoned and reused as necropolis due to the workability of the rock.

The Necropolis has suffered numerous and extensive interventions since its discovery. The first one was the adaptation of the necropolis for visits in 1885, including the construction of a trail, and planting of trees and gardens around the tombs. Nowadays this garden is considered one of the most deteriorating factors from the end of the 19th century until the end of the 20th century, because it affected the conservation of the tombs due to continuous irrigation and consequent percolation of water inside the tombs, in addition to the damage caused by roots (Benavente et al., 2011; Fernandez-Cortes et al., 2013).

Taking into account the cultural, artistic and religious importance of the Necropolis of Carmona, its preservation and conservation are a major issue, both from cultural and economic points of view. This importance emphasises the need to define accurate and sustainable intervention protocols based on a deep understanding of the environmental and/or anthropogenic-induced deterioration processes. The design of effective monument preservation and/or conservation strategies should be based on exhaustive *in situ* surveys and laboratory investigations (Heinrichs and Fitzner, 2000).

The main aim of this work consisted in the assessment of the conservation state of the Circular Mausoleum rock-cut tomb, including the identification of the main deteriorating agents. In addition, an intervention proposal for the preservation of the Circular Mausoleum was presented.

## 2. Methodology

### 2.1 Site description

The Necropolis of Carmona comprises a large number of tombs (about 600) excavated in a 30 m-thick Neogene sedimentary sequence. It is composed of decimeter-thick beds of poorly-sorted massive biocalcarenites (Fig. 1A,B). These are separated by lutitic and/or marly beds, ranging from millimeters to few centimeters thick and they are mostly discontinuous. This calcareous series is organized into four sequences, which in turn are divided into seven sub-sequences

1 or lithological units comprising the geological mapping of the site. Most tombs were  
2 collective mausoleums consisting of underground chambers accessed by a shaft.

3 The Circular Mausoleum is rectangular with a barrel vault and eleven niches carved  
4 on the walls (Fig. 1C). It is a small tomb, with less than 3 m of vertical  
5 development. The long side of the chamber has a N270° direction, with the  
6 entrance (a shaft) facing west. The tomb gets flooded by direct rainfall input  
7 through the shaft. At present, the walls and ceiling of the tomb are heavily  
8 deteriorated; only 50-60% of the inner surface is covered by mortars and stuccos.  
9

## 10 11 12 13 14 2.2. Materials characterization and alteration products

15 Circular Mausoleum building materials (host rock, mortars and stuccos) and  
16 alteration products (crusts, salt efflorescence and microbial colonization) were  
17 sampled and analysed. The mineralogical composition was analysed by powder X-  
18 ray diffraction in a Philips PW-1710/00 diffractometer using the Cu Ka radiation  
19 with a Ni filter and a setting of 40 kV and 40 mA. Data were collected and  
20 interpreted using the X Powder software package. The qualitative search-matching  
21 procedure was based on the ICDD-PDF2 database. A detailed study of the pore  
22 structure of host-rock, mortars and stuccos was carried out using nitrogen  
23 adsorption techniques, which provide specific surface area (SSA), volume fraction  
24 and pore size distribution in the micro-mesoporosity pore fraction. The  
25 determination of the SSA was carried out through the BET method in the relative  
26 pressure interval  $P/P_0 = 0.05-0.2$  by using an Autosorb-6 Quantachrome apparatus.  
27

28 To assess deterioration phenomena, the Circular Mausoleum was studied at the  
29 mesoscale by means of *in situ* description of weathering forms. Mapping of  
30 weathering forms were performed to register and evaluate the state of  
31 conservation on selected plans of the interior of the tomb. ICOMOS ICS glossary  
32 (2008) was used for weathering form terminology.  
33

## 34 35 36 37 38 39 40 41 42 43 2.3 Micro-environmental and climatic monitoring system

44 A micro-environmental monitoring system was installed inside the Circular  
45 Mausoleum to record the microclimate. The Data Acquisition System consisted of a  
46 HOBO-U12 data logger, with a set of four sensors to record air temperature, air  
47 relative humidity, temperature of the rock surface and light intensity. These  
48 parameters were recorded every 15 min from June 2007 to April 2009. In addition,  
49 it was used a HOBO Pro v2 data logger with built-in temperature and relative  
50 humidity sensors for air measurements (Onset Computer Corporation, Bourne, MA,  
51 USA). Air temperature was measured with an accuracy of  $\pm 0.2^\circ\text{C}$  over  $0^\circ$  to  $50^\circ\text{C}$ .  
52 The relative humidity sensor operated over a RH range from 0 to 100% with a  
53 minimum accuracy of  $\pm 3.5\%$  (above 95%). The rock-surface temperature was  
54 measured using a two thermocoupled sensor TMC20-HD (Onset Computer  
55  
56  
57  
58  
59  
60  
61  
62  
63  
64  
65

1 Corporation), with an accuracy of  $\pm 0.25^\circ$  at  $20^\circ\text{C}$ , inserted up to 2 cm inside the  
2 tomb wall and ceiling. Light intensity was measured using a pyranometer PYR-SA  
3 2,5V (Apogee Instruments, Logan, UT, USA) calibrated to measure total shortwave  
4 radiation up to  $1100\text{ W m}^{-2}$  (full sunlight) with an absolute accuracy of  $\pm 5\%$  and  
5 repeatability of  $\pm 1\%$ .  
6

7 Outdoor climate was measured by means of a weather station (HOBO Weather  
8 Station HWS, Onset Computer Corporation) which included a tipping-bucket rain  
9 gauge (S-RGB model) for rainfall measurements, a barometer S-BPA-CM10 providing  
10 average barometric pressure for each logging interval and a 12-bit Smart Sensor (S-  
11 THB model from Onset Computer Corporation) to measure the relative humidity  
12 and air temperature with an accuracy of  $\pm 0.2^\circ\text{C}$  over  $0^\circ$  to  $50^\circ\text{C}$ , and  $\pm 2.5\%$  from  
13 10% to 90% RH, to a maximum of  $\pm 3.5\%$  (above 95%).  
14  
15  
16  
17  
18  
19

#### 20 *2.4. Light flux and surface temperature measurements in the interior of the Tomb*

21 In order to define the spatial evolution of the daily and annual cycle of the  
22 perceived power of light and temperature in the inner surface of the tomb,  
23 measurements of both light flux and surface thermal radiation in the internal (non-  
24 exposed) areas of the Circular Mausoleum were achieved.  
25  
26

27 Luminous flux measurements were obtained with a digital light meter ISO-TECH,  
28 with a measuring range from 0.01 lux to 0.1 Klux, and an accuracy of  $\pm 3\%$   
29 (calibrated to standard incandescent lamp at colour temperature of 2856 K). The  
30 photodetector is a Silicon Photo Diode with a spectral response filter. Seventy six  
31 different sampling points and four different campaigns were performed: 1) on the  
32 evening of June 11, 2008; 2) on the morning of June 12, 2008; 3) on the evening of  
33 October 2, 2008; and 4) on the morning of January 28, 2009 (Fig. 2). These  
34 measurements were conducted close to the summer (sampling campaigns 1 and 2)  
35 and winter solstices (sampling campaign 4), and to equinox (sampling campaign 3).  
36 This roughly covered a whole year of luminous flux and allowed daily comparisons.  
37  
38  
39  
40  
41

42 The surface temperature was measured with a digital Pyrometer Trotec model TP8,  
43 with contact-free infrared surface thermometer. The sensor registers the thermal  
44 radiation emitted or reflected by the surface, with a correction parameter relative  
45 to the radiation emitted by each specific material. In this case, a standard emission  
46 factor of 0.95 for the studied materials was estimated. The measurement ranged  
47 from  $-50$  to  $+1000^\circ\text{C}$ , with a resolution of  $0.1^\circ\text{C}$ , a precision of  $\pm 1.5\%$  (in the  
48 range from  $-20$  to  $+200^\circ\text{C}$ ), an optical precision of 50:1, a spectral sensitivity of 6-  
49 14 microns and a minimum measure surface of 6 mm. In this case, six different  
50 campaigns were performed in the same 76 sampling points mentioned before (on  
51 the evening of October 18, 2007; on the evening of June 11, 2008; on the morning  
52 of June 12, 2008; on the morning and evening of October 2, 2008; and the morning  
53 of January 28, 2009). These sampling campaigns were performed close to the  
54  
55  
56  
57  
58  
59  
60  
61  
62  
63  
64  
65

1 summer solstice, three close to the equinox and another one close to the winter  
2 solstice.

3 A simple tomb 3D Computer Aided Design Model (CAD) was obtained from  
4 topographic information and completed together with detailed schemes (Bendala,  
5 1976), and then integrated in a 3D Geographic Information System (GIS)  
6 environment. This was the spatial context used to locate a georeferenced database  
7 of the sampling points and measurements. With these data, and applying a colour  
8 ramp depending on the individual values of light intensity and temperature, a  
9 schematic representation of the 3D evolution of both parameters in the interior of  
10 the tomb was achieved.

11 In order to calculate the duration of direct insolation in the Circular Mausoleum, a  
12 3D model of the main entrance of the tomb was obtained from existing  
13 topographies. From this elevation model, the duration of insolation in hours for the  
14 solstices and equinoxes were calculated (following algorithm and workflow from  
15 Dubayah and Rich, 1995, 1996; Fu and Rich 1999, 2000). These data allowed  
16 interpreting the spatial variation of the duration of insolation in the entrance area  
17 over an annual cycle and compare this with temperature and luminous flux  
18 measured in the interior of the tomb. Resulting spatial model in raster format was  
19 draped over 3D topographic model of the entrance of the tomb to evidence the  
20 spatial relations of the obtained duration of insolation values relative to the shape  
21 of the entrance.

## 2.5. *Identification of phototrophic microorganisms*

22 A sampling survey was conducted in May 2009 under the supervision of the Spanish  
23 authorities in charge of the Necropolis of Carmona. Six sampling areas exhibiting  
24 green biofilms were studied. These biofilms were gently scrapped, using a  
25 sterilized scalpel, and placed in sterile tubes for identification of phototrophic  
26 microorganisms by direct examination under light microscopy and culture methods.

27 Samples were inoculated on Petri plates containing solid BG11 culture medium and  
28 incubated at 20°C for four weeks. Features of individual species were observed  
29 using light microscopy equipped with a photographic camera. Taxonomic  
30 identification was based on morphological characters of colonies growing on the  
31 agar plates using identification keys (Ettl and Gärtner, 1995; Komárek and  
32 Anagnostidis, 1999, 2005).

33 The cultures of phototrophic microorganisms were analysed using molecular biology  
34 techniques for the identification of cyanobacteria and eukaryotes. DNA was  
35 extracted using FastDNA SPIN for Soil Kit (MP Biomedicals, Santa Ana, CA, USA) in  
36 conjunction with the FastPrep instrument, following the manufacturer's protocol.  
37 Amplifications of 16S and 18S rRNA gene sequences were performed by PCR using  
38 the cyanobacteria-specific primer pair, Cya106F and Cya781R (Nübel et al., 1997),  
39 and the Eukarya-specific primers, EukA and EukB (White et al. 1990), respectively.

1 PCR amplifications were performed using the following thermal conditions: 95°C  
2 for 2 min; 35 cycles of 95°C for 15 s, 60°C for 15 s (55°C for Eukarya-specific  
3 primers), 72 °C for 2 min; and a final step of 72°C for 10 min. DNA libraries of PCR  
4 amplified products were constructed using the TOPO-TA cloning kit (Invitrogen,  
5 Carlsbad, CA, USA) according to the manufacturer's recommendations. Plasmids  
6 were extracted with the JetQuick Plasmid Miniprep Spin Kit (Genomed, Löhne,  
7 Germany), following the manufacturer's protocol, and sequenced by Secugen  
8 Sequencing Services (CSIC, Madrid, Spain). Sequences were checked for chimera  
9 using the program Bellerophon (Huber et al., 2004) using a variety of window sizes  
10 (200-400 bp) and corrections. Sequences were aligned using the software package  
11 mothur (Schloss et al., 2009). Homology searches of the retrieved sequences were  
12 performed using the BLASTN algorithm (Altschul et al., 1990).  
13  
14  
15  
16  
17  
18

### 19 **3. Results**

#### 20 *3.1. Material properties*

21 The calcarenite host rock consisted of 75-85% calcareous grains (lamellibranchia  
22 predominating over oysters and small foraminifera). The remaining 15-25% was  
23 mainly quartz and trace amounts of phyllosilicates (smectite and illite). A matrix  
24 was rarely present in the calcarenite, and when present it consisted of very fine  
25 calcareous clay and lime-size grains. Calcite cement, with equant and drusy  
26 textures, was also rare and it was concentrated at the grain contacts.  
27  
28  
29  
30  
31

32 The calcarenite showed a complex porous media, with high porosity (24-33%) and  
33 polymodal pore size distribution. These pore space properties provided an  
34 important water condensation, capillary rise and salt weathering susceptibility.  
35 Moreover, calcarenite showed a very low mechanical strength, as revealed by axial  
36 compressive strength (5.90 MPa). A detailed description of the host rock physical  
37 properties can be found in Benavente et al. (2011), who studied the Postumius  
38 Tomb located in the same lithologic unit of Circular Mausoleum.  
39  
40  
41

42 The composition of the stuccos was calcite (70%), quartz (13%) and feldspar (17%);  
43 for fine-grained mortars the composition was calcite (77%) and quartz (23%); and  
44 for coarse-grained mortars calcite (46%), quartz (23%), gypsum (19%) and feldspar  
45 (12%) were identified. Calcite was found as aggregate and blinder in the studied  
46 stuccos and mortars.  
47  
48  
49

50 Stuccos and fine and coarse-grained mortars presented similar specific surface area  
51 (SSA) values (48.6, 41.2 and 53.7 m<sup>2</sup>/g, respectively), whereas the host rock  
52 showed the smallest SSA values (2.7 m<sup>2</sup>/g). Scanning electron microscopy  
53 observations showed an important volume fraction (porosity) in the studied  
54 materials, although the host rock presented largest pores than stuccos and  
55 mortars. Materials with high porosity but small mean pore size (for example,  
56 stuccos and mortars) presented higher SSA values than materials with a large mean  
57 pore radius (host rock).  
58  
59  
60  
61  
62  
63  
64  
65

### 3.2. Microclimatic characterization

The microclimate of the Circular Mausoleum and outdoor environmental parameters during the monitoring period are shown in Figure 3. In the hydrological cycle between September 2007 and August 2008, the exterior average temperature was 18.7°C, with monthly temperature variations ranging between 15.3°C (December) and 27.4°C (June). Annual average relative humidity was around 61% with a high level of short-term (daily) and seasonal fluctuations. The area was characterized by low annual rainfall (383.4 L/m<sup>2</sup>) with long periods of drought (June-August). The maximum rainfall was in spring (114.2 L/m<sup>2</sup> in April 2008) and autumn (71.4 L/ m<sup>2</sup> in November 2007).

The average air temperature inside the Circular Mausoleum during the same hydrological cycle (2007-2008) was 17.73°C with moderate values of both diurnal (5.62°C) and annual variation (18.54°C). The temperature evolution inside the tomb was parallel to the outer atmosphere but with temperature values significantly higher than those registered outside during winter (Fig. 3). A thermal equilibrium between the tomb's air and the surface of the inner walls and ceiling tended to be reached during winter months. This equilibrium suddenly changed in early spring when the rock temperature kept warmer than the air until early autumn. The evolution of the rock temperature at the two control points indicated a significant overheating of the ceiling (T2, annual average of 18.82°C with an annual oscillation of 17.28°C) compared to the walls (T1, annual average of 18.04°C with an annual oscillation of 16.68°C).

The relative humidity of the indoor air was moderately high, with an annual average value of 78.5% for the hydrological year 2007-2008. Its evolution was parallel to the exterior atmosphere (Fig. 3), with similar values during autumn and early winter (November to January). The greatest similarity of humidity conditions between inner and exterior air was related to ventilation favoured by the entry of cold, dense air from the outside during the coldest months. However, since February the internal humidity values were consistently above the external humidity (except for intervals with sharp external thermal dropping that caused new transient ventilation processes). The relative humidity differences between the inner and outer atmosphere were accentuated during the summer.

### 3.3. Condensation processes on the inner surfaces of the tomb

A detailed time-evolution of vapour condensation on the inner surfaces (e.g. rock-surface of ceiling) can be calculated in function of the microclimate conditions and pore structure properties of rock.

Figure 3 shows the amount of water condensing on the rock surface of ceiling per cubic meter of air within the tomb, during the monitoring period. Effective

1 condensation occurred when the relative humidity of the tomb air reached and  
2 remained above the threshold of 75%, as determined by Benavente et al. (2011) for  
3 this lithostratigraphic unit. This occurred mainly during the wetter and colder  
4 season, i.e. from October-November to end of April. The condensation was more  
5 intense when the tomb air temperature was above the rock-surface temperature  
6 (approximately 14-15°C). On the contrary, the effective condensation tended to be  
7 null when these environmental conditions change. Some sporadic and short  
8 intervals of condensation were registered during the warmer periods, even when  
9 the temperature of rock surface was higher than inner air; however this short-term  
10 condensation usually matched with some specific rainfall events causing humidity  
11 rises above 80%.

12 During wetter months (from October to April), the vapour condensation on the rock  
13 surface occurs 76% of days in each month, with a mean duration of 10.6 h per day.  
14 The daily-averaged amount of vapour condensation was estimated at 32 gH<sub>2</sub>O·m<sup>-3</sup>  
15 air and the subsequent alternation of condensation-evaporation was common every  
16 day (1.2 cycles on average).

#### 25 *3.4. Models of duration of insolation, light flux and surface temperature*

26 In general, direct potential insolation in the area occupied by the Roman  
27 Necropolis of Carmona was quite high and the overall climate conditions were  
28 warm the year round. In the area surrounding the studied tomb, the maximum  
29 direct potential insolation during the winter solstice reached 1842 W/m<sup>2</sup> with  
30 average values of 1027 W/m<sup>2</sup>. In the equinoxes this increased up to 4240 W/m<sup>2</sup>  
31 with average values of 3475 W/m<sup>2</sup>. During the summer solstice the maximum value  
32 reached 6039 W/m<sup>2</sup> with an average of 5792 W/m<sup>2</sup> (Fig. 4B). In the area were the  
33 tomb is located, which is flat and not protected from solar radiation, an important  
34 increase of the direct potential insolation from winter to summer was observed.  
35 This increase was more prominent from the spring equinox to the summer solstice  
36 than from the winter solstice to the spring equinox.

37 The duration of insolation models (Fig. 4A) showed that over a year changes in  
38 duration and location of direct insolation from the entrance to the interior of the  
39 tomb were very noticeable. During the winter solstice and the equinoxes, there  
40 was no direct insolation in the interior of the tomb and it was very limited in the  
41 uppermost area of the tomb entrance. In turn, during the summer solstice, the  
42 insolation reached a great area of the tomb interior through the shaft, from 1 to 3  
43 hours. On the roof of the tomb (40 cm thick), exposed the year round to direct  
44 insolation, an expected increase of insolation from 9 to 10 hours during winter  
45 solstice and equinoxes to more than 15 hours during the summer solstice was  
46 reported. The models of insolation for each season were consistent with the  
47 continuous records of light intensity performed inside the tomb, in particular with  
48 those registered on the east wall. From November to March light was undetectable  
49  
50  
51  
52  
53  
54  
55  
56  
57  
58  
59  
60  
61  
62  
63  
64  
65



(Fig. 4C); from middle March low levels of solar radiation started to be registered, increasing gradually till reaching their highest values in June-July.

The luminous flux for each sampling campaign displayed minor variations in both range of values and spatial distribution inside the tomb, which were related to its shape. In general, the luminous flux distribution inside the tomb depended on the season and time of the day, i.e. it was dependent on the relative position and inclination of the sun relative to the orientation of the tomb entrance. Incident light from the sun was reflected on the ground and walls of the entrance and on the roof of the tomb. Seasonal changes were noticeable and luminous flux increased from winter to summer mainly in the external zones of the tomb (Fig. 4A,B).

Surface temperature in the internal areas of the Circular Mausoleum was closely related to the outside air temperature. For all sampling campaigns, the minimum and maximum surface temperature values were 9.5 and 26.0°C, respectively, and the average values ranged from 11.6 to 23.04°C. The surface temperature variations in each campaign ranged from 3.5 to 7.1°C. In all data collection campaigns, temperature increases upward and inward from the tomb, the increasing ranging from 0.1 to 3°C. Daily evolution near the summer solstice clearly showed a broad area of steady temperatures and an increase towards the outside of the tomb (with an important cooling in the ceiling and walls). On the contrary, daily evolution in October (equinox) showed a cooling of a great part of the Circular Mausoleum, with higher stability in the most internal part of the tomb.

### 3.5. Weathering and biodeterioration

The Circular Mausoleum shows a severe alteration and different types of weathering forms can be distinguished. Visual examination of weathering forms comprising deposits and loss of material were abundant. In general, the most important weathering forms included loss and deformation of material (granular or crumbly disintegration, scaling, flaking, blistering, etc.) and surface modifications (efflorescence, encrustations and biological colonization) (Fig. 5).

The tomb walls displayed complex weathering patterns, represented by granular disintegration, crumbling or scaling. In some places (ceiling and niches) the surface recession was very significant (Fig. 5A), reaching several cm deep. In the ceiling, original mortars and stuccos were not preserved.

Deformation features, as bumps or blisters on the areas with stuccos, especially in the entrance area were relatively abundant. These were commonly associated with anthropogenic actions including graffiti scratches (Fig. 5D). Biological colonization was also influenced by vandalism episodes as observed in Figure 5E.

Diverse types of deposits have been recognized: (i) Crumbly fine-grained deposits on the surface of niche ledges (soiling), mainly composed of phototrophic

1 microorganisms and insect remains; (ii) salt efflorescence on walls, niches, rock,  
2 mortars, stuccos or restored materials (Fig. 5B,C), and (iii) different types of  
3 coatings and encrustations.

4 Efflorescence was mostly composed of gypsum and covered all types of substrates.  
5 Sodium sulfate salts were scarce. Efflorescence usually showed a powdery or fine-  
6 grained texture when directly covered the rock substrate (calcarenite) or coarse-  
7 grained mortar. On the surface of stuccos was also common the existence of a  
8 discontinuous deposit of gypsum crystals derived from the dissolution and  
9 recrystallization of gypsum efflorescences, giving a characteristic 'mikado'-like  
10 texture (Fig. 5C). Microcrystalline gypsum deposits also appeared as sub-  
11 efflorescences, usually under stucco or mortar layers. These deterioration patterns  
12 were solely visible at a mesoscale when the upper mortar or stucco layers were  
13 detached. Encrustations firmly adhered to the stone surface were generally  
14 observed. They showed different typologies from globulitic to thin smooth  
15 cryptocrystalline encrustations. Globulitic crusts formed smooth and rough surfaces  
16 on both mortars and stuccos and on calcarenitic substrate (Fig. 5B,C). Thin smooth  
17 cryptocrystalline encrustations were found covering mortars, and often drawing  
18 thread-like trails or paths (Fig. 5F,G). All of these phenomena were clearly due to  
19 precipitation processes, but formation mechanisms could be diverse. Globulitic  
20 botryoidal types were associated with seepage of infiltration water and/or  
21 condensation processes, whereas smooth cryptocrystalline encrustations were  
22 associated with flowing water (Fig. 5F, G).

23 Biological colonization was widespread inside the tomb. Microbial colonies  
24 distribution was highly controlled by the entrance orientation (facing west) and the  
25 distance to the ground. Photosynthetic-based colonization was particularly  
26 extended in holes and rough substrates (Fig. 5H). In the entrance (shaft) the walls  
27 were colonized by lichens (Fig. 5I), mosses, and phototrophic microorganisms.

28 Figures 6 and 7 show alteration maps, illustrating the spatial distribution of the  
29 major weathering forms developed on the inner arch and on the end (eastern) wall  
30 of the tomb.

31 On the wall of the inner arch (Fig. 6), the spatial distribution of the weathering  
32 forms exhibited a vertical zonation. Encrustations were much more widespread at  
33 the bottom than at the intermediate and upper zones, with efflorescence on the  
34 ceiling. Biologically induced deposits preferentially accumulated at the bottom.  
35 This zonation was not evident on the eastern wall (Fig. 7), where the nature of the  
36 substrate (composition and roughness), water condensation and laminar flow  
37 processes on the wall largely controlled the distribution of the weathering forms.  
38 On this wall, different phases of restoration involving mortars application were  
39 observed (Fig. 8). Some mortars were clear toned, coarse-textured, and well  
40 differentiated between them by the degree of alteration (blisters, efflorescence,  
41 and scabs). Recent mortars with brown coloration and finer grained texture also  
42 showed alteration, especially on the edges (deformations, efflorescence, etc.).

### 3.6. Phototrophic colonization

Figure 9 and Table 1 summarizes the characteristics of the samples analysed in the Circular Mausoleum tomb, where phototrophic microorganisms reached a particular relevance. While the shaft of access to the tomb had direct insolation and the walls were mainly coated by the lichen *Dirina massiliensis* (Fig. 5I), the arch and the interior of the tomb were populated by cyanobacteria and algae. The walls near the ground level were characterized by the predominance of chlorophyta over cyanobacteria (L12, MC1 and 2), while cyanobacteria were mostly present on or near the ceiling (MC3, MC4 and MC5). Direct microscopic observations of the samples identified among the chlorophyta *Muriella terrestris* and *Muriella* sp., while the cyanobacteria were represented by *Cyanothamnos* sp., *Chroococcidiopsis* sp., *Symplocastrum friesii*, *Leptolyngbya* spp., *Gloeocapsa rupestris*, and *Scytonema* sp. When the samples were cultured in the laboratory, the dominant species in the plates were the chlorophyta *Chlorella vulgaris* and *Ctenocladus circinnatus*, and the cyanobacteria *Symplocastrum friesii*, *Leptolyngbya* spp., *Chroococcidiopsis* sp. and *Gloeocapsa rupestris*. Additional molecular studies revealed that *Loriellopsis cavernicola* was present in sample L12, *Jenufa minuta* in samples MC1 and MC2, and *Leptolyngbya* sp. and *Oculatella* sp. in sample MC4.

## 4. Discussion

The Circular Mausoleum showed a high degree of deterioration. The nature of the building materials and the numerous interventions works in the tomb increased damages promoted by high humidity and condensation rates. In fact, mineralogical, textural and petrophysical characterization of the host rock pointed out to a high susceptibility to decay for this calcarenite, which corroborated the similar nature of host rocks of the Circular Mausoleum and the previously studied Postumius Tomb, both in the same sedimentary sequence (Benavente et al., 2011). Deterioration patterns were observed in the calcarenite host rock and stuccos/mortars substrates. They comprised a varied and abundant array of damages, including material detachment (scaling, flaking, granular disintegration), surface discoloration, deposits (efflorescence and crusts), and biological colonization (Figs. 6 and 7).

The deterioration processes observed in the tomb can be summarized as:

- Dissolution/crystallization of salts on the porous system (host rock, stuccos and mortars) due to: (i) the presence of liquid water (flooding or condensation) and capillary absorption kinetics, and (ii) daily and seasonal relative humidity variations in the tomb.
- Dissolution of calcarenite substrate, which caused loss of cohesion and subsequent granular or crumbly disintegration. Both water (liquid or vapour)

1 and CO<sub>2</sub> (air, natural and anthropogenic soil covering the rock) were the  
2 main factors in the dissolution of the carbonate rock.

- 3 • Anthropogenic actions involving archaeological excavations and vandalism  
4 (engraving and scratching) resulting in important mechanical damages on the  
5 surface and loss of substrate material.
- 6 • Biofilm development and subsequent biodeterioration. An important  
7 biological activity by phototrophic microorganisms was promoted due to high  
8 humidity, natural dim light and mineral availability.

9  
10  
11  
12 The combined action of these alteration processes gave rise to the current severe  
13 deterioration state of the Circular Mausoleum, in which water was the principal  
14 agent of deterioration.

15  
16  
17 The seasonal and daily cycles of heating-cooling and the important direct solar  
18 radiation over the tomb roof causing overheating, implied the decreasing of air  
19 relative humidity and increasing of building material temperatures. These cycles  
20 not only enhanced weakness of the joint host rock-mortar by differential thermal  
21 stress but also disintegration of the mortars, stuccos and rock, and crystallization-  
22 dissolution of salts. Wetting-drying cycles, responsible of salt precipitation, were  
23 particularly evident at the rock-mortar interface due to different pore size  
24 distributions.

25  
26  
27 Pore structure characterization showed that these materials presented a significant  
28 porosity. SSA revealed that stuccos and mortars had thin pores whereas the host  
29 rock showed large mean pore radius. SSA is directly related to porosity and  
30 inversely related to pore size (Benavente et al., 2007; Benavente, 2011) and  
31 therefore, provides pore structure information related to decay mechanisms. Thus,  
32 high SSA values imply a high susceptibility to salt weathering (Benavente et al.,  
33 2007), capillary stress (Benavante et al., 2008), high capacity to water  
34 condensation and retention within porous materials, and consequently, high  
35 bioreceptivity (Sanchez-Moral et al., 2005; Miller et al. 2012). In addition, the  
36 presence of a water film might decrease the free surface energy of the material,  
37 decreasing its strength. The material aptitude to water retention had also an  
38 impact on the calcite dissolution, promoting material detachment (granular  
39 disintegration, scaling, etc.).

40  
41  
42 The high relative humidity and the petrophysical properties of the substrates  
43 promoted water condensation inside the tomb, especially in winter (Benavente et  
44 al., 2011; Fernandez-Cortes et al., 2013). The procedure to calculate the amount  
45 of water condensing on an exposed rock/soil surface was extensively described by  
46 Fernandez-Cortes et al. (2013). It depends on: 1) the evolution over time of the  
47 differences in vapour pressure between air and the rock/soil surface, and 2) the  
48 control exerted by the rock porous system based on laboratory experiments to  
49 calculate water adsorption curves of rock/soil samples at different relative  
50 humidity. The effective condensation occurs when vapour pressure in the air is

1 higher than on the rock surface, which is corrected by a threshold of relative  
2 humidity, above which water condensation is more active due to the presence of a  
3 pore structure and dissolved salts. It has been previously tested on laboratory for  
4 several host rock samples from the same lithostratigraphic unit where the tomb  
5 was carved, revealing a relative humidity threshold for the tomb air of 70-75%,  
6 from which the amount of water adsorbed by the porous surface system  
7 significantly increased (Benavente et al., 2011).  
8  
9

10 In summer, the lack of air ventilation due to the narrow vertical entrance (shaft) of  
11 the tomb resulted in the entrapment of cold and wet air from the outside, causing  
12 a moisture gradient between the inner floor and ceiling which activated water  
13 capillary rise through tomb walls and promotes biological colonization.  
14  
15

16 The colonization of rocks by phototrophic communities in subterranean  
17 environments is often associated with sites of high humidity and low light intensity,  
18 as occurring in the Circular Mausoleum. However the combination of other  
19 different ecological factors, such a temperature and nutrient availability may also  
20 influence the distribution of such microorganisms due to specific adaptations to the  
21 conditions prevailing in a niche (Figs. 6 and 7). Most of the phototrophic  
22 microorganisms found are ubiquitous in subterranean environments, but a  
23 considerable number of species are endemic forms or even new species that in the  
24 last few years where described for the first time (Lamprinou et al. 2011).  
25  
26  
27  
28  
29

30 Colonization of subterranean environments by phototrophic microorganisms  
31 depends on light, water and nutrient availability. In this tomb several sources or  
32 nutrients are available for microbial growth and biofilms: i) organic carbon and  
33 soluble salts carried out by rainwater and flooding of the tomb in raining seasons,  
34 ii) soluble salts and dissolved organic carbon brought by ascending capillarity in  
35 warm seasons, iii) activity of insects and small animals (spiders, geckos, etc.),  
36 which contributes to the dispersion of microorganisms all around the tomb walls  
37 and ceiling. Although this study was focused on phototrophic microorganisms,  
38 heterotrophic microorganisms such as bacteria and fungi also form part of the  
39 biofilms (Lappin-Scott and Costerton, 1995).  
40  
41  
42  
43

44 In the past some small tombs from this Necropolis were investigated and a  
45 calcifying cyanobacterial community represented by *Scytonema julianum* and  
46 *Geitleria calcarea* was identified (Ariño et al. 1997). In some other tombs the  
47 studies were focused on the lichenic community (Ariño and Saiz-Jimenez, 1997).  
48  
49

50 In the Circular Mausoleum, calcifying cyanobacteria were rarely observed and only  
51 *Scytonema* sp. was identified by direct microscopic observation (Table 1). In this  
52 tomb, spatial variations in light intensity and humidity may even led to species  
53 segregation in adjacent materials. In fact, the particular microclimate conditions in  
54 this tomb gave rise to special niches for phototrophic microorganisms. Chlorophyta  
55 were common near the ground level due to the high moisture content the year  
56 round. In contrast, cyanobacteria were especially successful on the ceiling and  
57  
58  
59  
60  
61  
62  
63  
64  
65

1 adjacent walls, where abundant cracks and holes were present with very low light  
2 intensity. On the dry walls receiving sunlight (near the tomb entrance) or on the  
3 ceiling, reaching high temperatures due to insolation, the presence of  
4 cyanobacteria was remarkable which indicates a better adaptation to dryness.  
5 Therefore, there is a clear trend in the ecology of phototrophic microorganisms in  
6 this tomb.  
7

8  
9 The resistance of cyanobacteria to extreme environmental conditions has been  
10 reported by several authors (Ortega-Calvo et al, 1992; Ariño and Saiz-Jimenez,  
11 1996). Particularly, the genus *Chroococidiopsis* is characterized by the ability to  
12 survive prolonged desiccation periods, dominating the most extreme arid habitats  
13 (Billi et al., 2000). Therefore it is not surprising the finding of *Chroococidiopsis* on  
14 the ceiling of this tomb and on the upper parts of the walls subjected to high  
15 insolation in summer. Some other cyanobacteria, such as *Gloeocapsa rupestris*,  
16 *Symplocastrum friesii*, *Leptolyngbya* sp. and *Oculatella* sp., have thick  
17 mucilaginous sheath and cells are encased in a protective extracellular matrix  
18 composed predominantly of polysaccharides. This matrix protects the cells from  
19 desiccation (Büdel et al. 2009; Albertano, 2012).  
20

21  
22 It should be noticed that in Table 1 some differences were observed between the  
23 phototrophic microorganisms directly identified from the fresh sample and those  
24 identified after culturing. These differences were due to the fact that some  
25 cyanobacteria and algae were more prone to grow in culture media than others and  
26 in this way the most abundant species identified in cultures could not be  
27 necessarily those present in fresh samples collected from the tomb.  
28

29  
30 For taxonomical identification of cyanobacteria, the establishment of genera is  
31 based on both the molecular evaluation of genotypes and phenotypic characters,  
32 which are continually corrected and updated (Hoffmann et al., 2005; Komárek et  
33 al., 2014). Different hypogean-adapted species with morphological similarity could  
34 be attributed to highly convergent forms that can mask taxonomic relationships  
35 and morphologically similar types are indistinguishable or barely distinguishable.  
36 Some species found in the Circular Mausoleum represent an example of shared  
37 morphology in genetically different strains such as the genera *Chlorella* and  
38 *Jenufa*. In fact, we observed *Muriella terrestris* in the samples collected while  
39 after a few weeks of culture the Petri dish was dominated by *Chlorella vulgaris*. In  
40 2011 the genus *Jenufa* was separated from *Chlorella* based on molecular  
41 evidences, although morphologically both genera were similar and even similar to  
42 some *Muriella* (Nemcová et al., 2011).  
43

44  
45 *Loriellopsis cavernicola* and *Iphinoe spelaeobios* represent an example of shared  
46 morphology in genetically different strains, as well. Both are components of  
47 natural populations in subterranean environments with a disjointed and worldwide  
48 distribution (Lamprinou et al. 2011), where dim light seems to be a major stress  
49 factor. *Loriellopsis cavernicola* was found in a previous sampling in the Circular  
50 Mausoleum and in Servilia tomb, at some 100 m from the former. *Iphinoe*  
51  
52  
53  
54  
55  
56  
57  
58  
59  
60  
61  
62  
63  
64  
65

1 *spelaeobios* was further identified in this tomb associated with some  
2 actinobacterial niches dominated by *Streptomyces* spp. (data not published), which  
3 produce a violet diffusible pigment (Fig. 5E), but not found in the samples studied  
4 in Table 1. It should be noted that sampling on different time periods and niches in  
5 this tomb can provide different identifications depending on ecological adaptations  
6 and physiological status (dry substrate in summer and wet in winter).  
7

8  
9 The molecular data from the Circular Mausoleum showed representatives of two  
10 genera *Leptolyngbya* and *Oculatella* with a similarity of 99% (sample MC4). Direct  
11 observation of fresh samples and cultures revealed the presence of the  
12 cyanobacteria *Symplocastrum friesii* and *Leptolyngbya* sp. The genus *Leptolyngbya*  
13 is heterogeneous and polyphyletic with a high genotypic diversity hidden behind  
14 their simple morphology and minute dimensions (Anagnostidis and Komárek, 1988).  
15 This genus was erected to accommodate several old filamentous species of the  
16 genera *Lyngbya*, *Phormidium* and *Plectonema* and defined as a wide natural cluster  
17 (genotype) (Komárek et al. 2014). In nature, they form irregular clusters or mats  
18 and most of them show high photosynthetic efficiency as an adaptation to  
19 hypogean habitats and ability to growth heterotrophically (Roldán and Hernández  
20 Mariné 2009; Albertano 2012).  
21  
22

23  
24 The genus *Oculatella* (Zammit et al., 2012) and the species *Oculatella subterranea*,  
25 was established after the study of some Roman and Maltese catacombs applying a  
26 combination of both morphological and molecular data. The main morphological  
27 features of *Oculatella* are the red-purple coloration of cells and the presence of an  
28 orange photoreceptive structure at the trichomes tips. *Oculatella* sp. was  
29 identified in three different Carmona tombs (Three Doors, Elephant and Servilia)  
30 using molecular tools, but was only morphologically identified in Servilia tomb,  
31 where exhibited the characteristic purple-red colour of the trichomes and the  
32 orange tip (data not published).  
33  
34  
35  
36  
37  
38  
39  
40

## 41 **5. Conclusions and recommendations**

42  
43  
44

45 This study showed that the Circular Mausoleum has suffered from a severe  
46 deterioration since its discovery and exhumation. The nature of the host rock, a  
47 soft calcarenite, and the intervention works over time enhanced the observed  
48 damage.  
49  
50

51 Since its construction, the tomb has passed through several stages in which  
52 alteration processes were varied in types and degree of intensity (Fig. 10). After  
53 the discovery of the Circular Mausoleum, intervention works caused changes in the  
54 tomb access and in the interior, which represented a radical modification in their  
55 environmental conditions (Fig. 10A-C). The chamber opening through the eastern  
56 side and excavation and partial destruction of the superstructure (dome) expedited  
57 the libation conduit (Fig. 10C). A subsequent intervention resulted in the opening  
58  
59  
60  
61  
62  
63  
64  
65

1 of the original entrance to the chamber and the closure of the former entrance  
2 (eastern wall/ceiling and libation conduit). In this work, the dome was re-filled,  
3 probably reusing the excavation materials, resulting in a lower degree of  
4 compaction than the original material, thereby decreasing its insulating capacity,  
5 which resulted in a significant heating of the tomb (Fig. 10D).  
6

7 According to information from the Archaeological Site of Carmona Directorate,  
8 despite the extensive duration of phases B and C of Figure 10, the state of  
9 conservation of the tomb was significantly better than at present. As a  
10 consequence of the numerous interventions suffered since its discovery, this tomb  
11 currently presents a high degree of moisture, a high rate of condensation and  
12 significant overheating in the ceiling, which causes a sharp temperature gradient  
13 inside the tomb, with net air stratification.  
14  
15  
16

17 The preventive measures to be carried out in order to minimize the deterioration  
18 processes currently affecting the tomb should aim to reduce the amount of water  
19 and its residence time in the tomb. Based on deterioration diagnosis, effective  
20 corrective actions can be proposed. On a short-term, local scale, these preventive  
21 steps should include: (i) Protection of the tomb entrance to prevent the entry of  
22 water by direct rainfall or by runoff (Fig. 10D). This protective shelter should allow  
23 ventilation of the tomb and could be disassembled in summer; (ii) Reopening the  
24 conduit for libations and removal of organic and inorganic materials accumulated in  
25 the tomb ground as a result of entrainment and deposition by surface runoff. These  
26 measures would increase the rate of air exchange and would reduce the water  
27 availability in the tomb, the main deterioration agent.  
28  
29  
30  
31  
32  
33  
34  
35

### 36 **Acknowledgements**

37 This research was funded by the Consejería de Cultura, Junta de Andalucía, the  
38 Spanish Ministry of Science and Innovation project CGL2010-17183, and the  
39 program Torres Quevedo (PTQ 13-06296 and PTQ 12-05601). We thank the staff of  
40 Archaeological Site of Carmona for their collaboration.  
41  
42  
43  
44

### 45 **References**

- 46 Albertano, P., 2012. Cyanobacterial biofilms in monuments and caves. In: Whitton,  
47 B.A. (ed.), *Ecology of Cyanobacteria II: Their Diversity in Space and Time*,  
48 Dordrecht: Springer, pp. 317-343.  
49  
50  
51 Altschul, S.F., Gish, W., Miller, W., Myers, E.W., Lipman, D.J., 1990. Basic local  
52 alignment search tool. *J. Mol. Biol.* 215, 403-410.  
53  
54  
55 Ariño, X., Saiz-Jimenez, C., 1996. Factors affecting the colonization and  
56 distribution of cyanobacteria, algae and lichens in ancient mortars. In:  
57 Riederer, J. (ed.), *8th International Congress on Deterioration and Conservation*  
58 *of Stone*, vol. 2, pp. 725-731.  
59  
60  
61  
62  
63  
64  
65



- 1 Ariño, X., Saiz-Jimenez, C., 1997. Deterioration of the Elephant tomb (Necropolis  
2 of Carmona, Seville, Spain). *Int. Biodeter. Biodegr.* 40, 233-239.
- 3 Ariño, X., Hernandez-Marine, M., Saiz-Jimenez, C., 1997. Colonization of Roman  
4 tombs by calcifying cyanobacteria. *Phycologia* 36, 366-373.
- 5  
6 Benavente D., 2011. Why pore size is important in the deterioration of porous  
7 stones used in the built heritage? *Macla* 15, 41-42.
- 8  
9 Benavente D., Cueto N., Martínez-Martínez J., García-del-Cura M.A., Cañaveras  
10 J.C., 2007. Influence of petrophysical properties on the salt weathering of  
11 porous building rocks. *Environ. Geol.* 52, 197-206.
- 12  
13 Benavente D., Cultrone G., Gómez-Heras M., 2008. The combined influence of  
14 mineralogy, hydric and thermal properties in the durability of porous building  
15 stones. *Eur. J. Mineral.* 20, 673-685.
- 16  
17 Benavente, D., Sanchez-Moral, S., Fernandez-Cortes, A., Cañaveras, J.C., Elez, J.,  
18 Saiz-Jimenez, C., 2011. Salt damage and microclimate in the Postumius Tomb,  
19 Roman Necropolis of Carmona, Spain. *Environ. Earth Sci.* 63, 1529-1543.
- 20  
21 Bendala, G., 1976. La necrópolis romana de Carmona (Sevilla). Diputacion de  
22 Sevilla, 140 p.
- 23  
24 Billi, D., Imre Friedmann, E., Hofer, K.G., Grilli Caiola, M., Ocampo-Friedmann, R.,  
25 2000. Ionizing-radiation resistance in the desiccation-tolerant cyanobacterium  
26 *Chroococcidiopsis*. *Appl. Environ. Microbiol.* 66, 1489-1492.
- 27  
28 Bourrelly, P., 1990. Les algues d'eau douce - Initiation à la systématique, I: Les  
29 Algues Vertes. N. Boubée, Paris, 572 p.
- 30  
31 Büdel, B., Darienko, T., Deutschewitz, K., Dojani, S., Friedl, T., Mohr, K.I.,  
32 Salisch, M., Reisser, W., Weber, B., 2009. Southern African biological soil crusts  
33 are ubiquitous and highly diverse in drylands, being restricted by rainfall  
34 frequency. *Microb. Ecol.* 57, 229-247.
- 35  
36 Dubayah, R., Rich, P.M., 1995. Topographic solar radiation models for GIS. *Int. J.*  
37 *Geogr. Inf. Syst.* 9, 405-413.
- 38  
39 Dubayah, R., Rich, P.M., 1996. GIS-based solar radiation modeling. In: Goodchild,  
40 M.F., Steyaert, L.T., Parks. B.O., Johnston, C., Maidment, D., Crane, M.,  
41 Glendinning, S. (eds.). *GIS and Environmental Modelling: Progress and Research*  
42 *Issues*. Fort Collins: GIS World Books, pp. 129-134.
- 43  
44 Ettl, H., Gärtner, G., 1995. *Syllabus der Boden, Luft und Flechtenalgen*. Stuttgart:  
45 G. Fischer, 721 p.
- 46  
47 Fernandez-Cortes, A., Benavente, D., Cuezva, S., Cañaveras, J.C., Alvarez-Gallego,  
48 M., Garcia-Anton, E., Soler, V., Sanchez-Moral, S., 2013. Effect of water vapour  
49 condensation on the radon content in subsurface air in a hypogeal inactive-  
50 volcanic environment in Galdar cave, Spain. *Atmos. Environ.* 75, 15-23.
- 51  
52  
53  
54  
55  
56  
57  
58  
59  
60  
61  
62  
63  
64  
65

- 1 Fu, P., Rich, P.M., 1999. Design and implementation of the Solar Analyst: An  
2 ArcView extension for modeling solar radiation at landscape scales. In:  
3 Proceedings of the 19th Annual ESRI User Conference. San Diego, CA: ESRI.  
4 Retrieved July 9, 2008, from [http://gis.esri.com/library/userconf/  
5 proc99/proceed/papers/pap867/p867.htm](http://gis.esri.com/library/userconf/proc99/proceed/papers/pap867/p867.htm)  
6
- 7 Fu, P., Rich, P.M., 2000. The Solar Analyst 1.0 User Manual. Lawrence: Helios  
8 Environmental Modeling Institute, 49 p.  
9
- 10 Heinrichs, K., Fitzner, B., 2000. Deterioration of rock monuments in Petra/Jordan.  
11 In: Fassina, V. (ed.), Proceedings of the 9th International Congress of the  
12 Deterioration and Conservation of Stone, vol. 2, Amsterdam: Elsevier, pp. 53-  
13 61.  
14
- 15 Hoffmann, L., Komárek, J., Kastovsky, J., 2005. System of cyanoprokaryotes  
16 (cyanobacteria)-state in 2004. *Algol. Stud.* 117, 95-115.  
17
- 18 Huber, T., Faulkner, G., Hugenholtz, P., 2004. Bellerophon: a program to detect  
19 chimeric sequences in multiple sequence alignments. *Bioinformatics* 20, 2317-  
20 2319.  
21
- 22 ICOMOS-ICS, 2008. Illustrated glossary on stone deterioration pattern.  
23 [http://international.icomos.org/publications/monuments\\_and\\_sites/15/pdf/Mo-  
24 numents\\_and\\_Sites\\_15\\_ISCS\\_Glossary\\_Stone.pdf](http://international.icomos.org/publications/monuments_and_sites/15/pdf/Monuments_and_Sites_15_ISCS_Glossary_Stone.pdf)).  
25
- 26 Komárek, J., Anagnostidis, K., 1999. Cyanoprokaryota 1. Chroococcales. In: Ettl,  
27 H., Gärtner, G., Heynig, H., Mollenhauer, D. (eds.), Süßwasserflora von  
28 Mitteleuropa, 19/1, Heidelberg: Spektrum, 548 p.  
29
- 30 Komárek, J., Anagnostidis, K., 2005. Cyanoprokaryota 2. Oscillatoriales. In: Büdel,  
31 B., Krienitz, L., Gärtner, G., Schagerl, M. (eds.) Süßwasserflora von  
32 Mitteleuropa 19/2. Heidelberg: Elsevier, 759 p.  
33
- 34 Komárek J., Kaštovský J., Mareš J., Johansen J.R., 2014. Taxonomic classification  
35 of cyanoprokaryotes (cyanobacterial genera) 2014, using a polyphasic approach.  
36 *Preslia* 86, 295-335.  
37
- 38 Laiz, L., Miller, A.Z., Jurado, V., Akatova, E., Sanchez-Moral, S., Gonzalez, J.M.,  
39 Dionisio, A., Macedo, M.F., Saiz-Jimenez, C., 2009. Isolation of *Rubrobacter*  
40 strains from biodeteriorated monuments. *Naturwissenschaften* 96, 71-79.  
41
- 42 Lamprinou, V., Hernández-Mariné, M., Canals, T., Kormas, K., Economou-Amilli,  
43 A., Pantazidou, A., 2011. Morphology and molecular evaluation of *Iphinoe*  
44 *spelaeobios* gen. nov., sp. nov. and *Loriellopsis cavernicola* gen. nov., sp. nov.,  
45 two stigonematalean cyanobacteria from Greek and Spanish caves. *Int. J. Syst.*  
46 *Evol. Microbiol.* 61, 2907-2915.  
47
- 48 Lappin-Scott, H.M., Costerton, J.W., 1995. Microbial biofilms. Cambridge:  
49 University Press, 315 p.  
50  
51  
52  
53  
54  
55  
56  
57  
58  
59  
60  
61  
62  
63  
64  
65

- 1  
2  
3  
4  
5  
6  
7  
8  
9  
10  
11  
12  
13  
14  
15  
16  
17  
18  
19  
20  
21  
22  
23  
24  
25  
26  
27  
28  
29  
30  
31  
32  
33  
34  
35  
36  
37  
38  
39  
40  
41  
42  
43  
44  
45  
46  
47  
48  
49  
50  
51  
52  
53  
54  
55  
56  
57  
58  
59  
60  
61  
62  
63  
64  
65
- Maier Allende, J., 1999. Jorge Bonsor (1885-1930). Un académico correspondiente de la Real Academia de la Historia y de la Arqueología Española. Madrid: Real Academia de la Historia, 300 p.
- Miller, A.Z., Sanmartin, P., Pereira-Pardo, L., Dionisio, A., Saiz-Jimenez, C., Macedo, M.F., Prieto B., 2012. Bioreceptivity of building stones. A review. *Sci. Total Environ.* 426, 1-12.
- Nemcová, Y., Eliás, M., Skaloud, P., Hodac, L., Neustupa, J., 2011. *Jenufa* gen. nov.: A genus of coccoid green algae (*Chlorophyceae, incertae sedis*) previously recorded by environmental sequencing. *J. Phycol.* 47, 928-938.
- Nübel, U., Garcia-Pichel, F., Muyzer, G., 1997. PCR primers to amplify 16S rRNA genes from cyanobacteria. *Appl. Environ. Microbiol.* 63, 3327-3332.
- Ortega-Calvo, J.J., Hernández-Marine, M., Saiz-Jimenez, C., 1992. Experimental strategies for investigation stone algal colonization. In: J. Delgado Rodrigues, F. Henriques and F. Telmo Jeremias (eds.), 7th International Congress on Deterioration and Conservation of Stone. Lisboa: Laboratorio Nacional de Engenharia Civil, pp. 541-549.
- Piñar, G., Saiz-Jimenez, C., Shabereiter-Gurtner, C., Blanco-Varela, M.T., Lubitz, W., Rölleke, S., 2001. Archaeal communities in two disparate deteriorated ancient wall paintings: detection, identification and temporal monitoring by DGGE. *FEMS Microbiol. Ecol.* 37, 45-54.
- Rada y Delgado, J.D., 1885. Necrópolis de Carmona: Memoria escrita en virtud de acuerdo de las Reales Academias de la Historia y de Bellas Artes de San Fernando. Madrid: Real Academia de la Historia, 179 p.
- Roldán M., Hernández-Mariné M., 2009. Exploring the secrets of the three-dimensional architecture of phototrophic biofilms in caves. *Int. J. Speleol.* 38, 41-53.
- Sanchez-Moral, S., Luque, L., Cuezva, S., Soler, V., Benavente, D., Laiz, L., Gonzalez, J.M., Saiz-Jimenez, C., 2005. Deterioration of building materials in Roman catacombs: the influence of visitors. *Sci. Total. Environ.* 349, 260-276.
- White, T.J., Bruns, T., Lee, S., Taylor, J., 1990. Amplification and direct sequencing of fungal ribosomal RNA genes for phylogenetics. In: Innis, M.A., Gelfand, D.H., Sninsky, J.J., White, T.J. (eds.), *PCR protocols: A guide to Methods and Applications*. New York: Academic Press, pp. 315-322.
- Zammit, G., Billi, D., Albertano, P., 2012. The subaerophytic cyanobacterium *Oculatella subterranea* (Oscillatoriales, Cyanophyceae) gen. et sp. nov.: a cytomorphological and molecular description. *Eur. J. Phycol.* 47, 341-354.

## FIGURE CAPTIONS

1  
2 Figure 1. A. Location of Circular Mausoleum (CM) in the Carmona Necropolis  
3 Archaeological Site. B. The Circular Mausoleum in the lithostratigraphic profile. C.  
4 3D-scheme of the Circular Mausoleum.  
5

6 Figure 2. Variation in light intensity measured in the morning of January 28, 2009.

7  
8 Figure 3. Temporal evolution of the external climatic conditions and main  
9 microclimatic parameters inside the tomb (temperature and relative humidity of  
10 air, rock-surface temperature and effective condensation process in the rock  
11 surface of the ceiling.  
12  
13

14 Figure 4. A. Evolution of the modelled duration of the insolation at the entrance of  
15 the tomb (3D simplified model) during an annual cycle. B. Summer solstice model  
16 of the direct insolation. C. Evolution of the light intensity recorded at the Tomb of  
17 Circular Mausoleum during the annual cycle April 2008 - April 2009.  
18  
19

20 Figure 5. A. Gravitational crusts near to niche edges probably associated with the  
21 drain of condensation water. B. Globulitic encrustation. C. Detail of globulitic  
22 precipitates and associated microorganisms (cyanobacteria and algae). D. Flakes  
23 and blisters associated with anthropogenic scratches. E. Details of how a scratch  
24 can transport spores and induce a microbial colonization characterized by a violet  
25 diffusible pigment. F. Green biofilms in trails related to gravitational  
26 encrustations. Colonies must be associated to water condensation and subsequent  
27 runoff processes. G. Details of vertically-arranged green biofilms in association to  
28 gravitational encrustations. Like the latter, the settlements should be associated  
29 with processes of condensation and water runoff. H. Phototrophic biofilms on rough  
30 substrate (due to spalling, disaggregation). I. Lichens (*Dirina massiliensis*) in the  
31 entrance of the tomb (shaft).  
32  
33  
34  
35  
36  
37

38 Figure 6. Distribution of weathering forms on the inner arch wall of the Circular  
39 Mausoleum.  
40

41 Figure 7. Distribution of weathering form on the eastern wall of the Circular  
42 Mausoleum.  
43  
44

45 Figure 8. Different types of restoration materials on the inner wall of the Circular  
46 Mausoleum. A. Rough, gray-colored, highly altered substrate (blisters,  
47 efflorescences, botryoidal crusts, etc.). A'. Rough, gray-colored, slightly altered  
48 substrate. B. Brown-colored substrate with edges alterations (efflorescences and  
49 flakes).  
50  
51

52 Figure 9. Phototrophic colonization in the Circular Mausoleum. A. Green biofilm on  
53 the eastern wall of the tomb, near the ground. B. Thin green biofilm on the eastern  
54 wall. C. Thin green biofilm on the left side of the inner arch. D) Green biofilm on  
55 the tomb ceiling. E. Green biofilm at the entrance. F. Green biofilm on the  
56 northern wall, near the tomb ceiling.  
57  
58  
59  
60  
61  
62  
63  
64  
65

Figure 10. Evolution stages of the Circular Mausoleum. A. Roman phase. The tomb was in use. B. Burial phase. The tomb was abandoned. Between the abandoned state and its discovery, the tomb was buried preventing flooding phenomena and air circulation. C. Discovery phase (last decades of 19th century). It comprised opening of the tomb through the eastern wall and destruction of structural elements. D. Present stage. Restoration of the dome structure (roof). Liquid water (flooding or condensation) and capillary movement during raining periods are frequent. High RH, temperature gradient, and condensation in the tomb are experienced during summer. E. Proposed corrective phase.

1  
2  
3  
4  
5  
6  
7  
8  
9  
10  
11  
12  
13  
14  
15  
16  
17  
18  
19  
20  
21  
22  
23  
24  
25  
26  
27  
28  
29  
30  
31  
32  
33  
34  
35  
36  
37  
38  
39  
40  
41  
42  
43  
44  
45  
46  
47  
48  
49  
50  
51  
52  
53  
54  
55  
56  
57  
58  
59  
60  
61  
62  
63  
64  
65

## Table

[Click here to download Table: Table 1.docx](#)

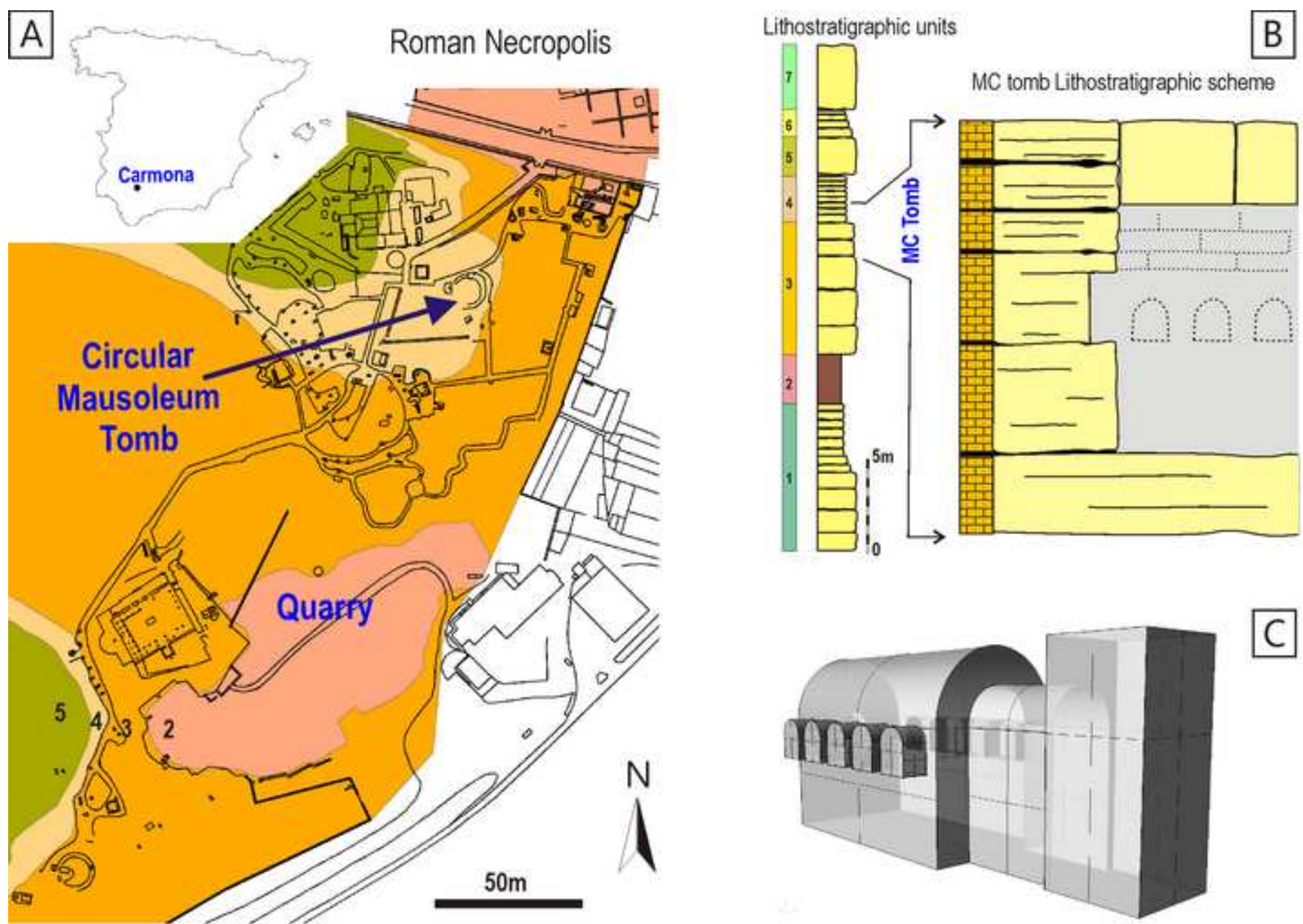
Table 1. Phototrophic colonization in the Circular Mausoleum

Sample	Sample description	Phototrophic microorganisms identified on fresh samples	Dominant phototrophic microorganisms identified after culturing	Molecular identification of cultures, accession number and % similarity
L12	Green biofilm developing on the rough substrate from the eastern wall of the tomb, near the ground (Fig. 9A).	<i>Muriella</i> sp. <i>Cyanothamnos</i> sp. <i>Chroococciopsis</i> sp.	<i>Chlorella vulgaris</i> <i>Symplocastrum friesii</i>	<i>Loriellopsis cavernicola</i> NR117881 (91%)
MC1	Thin green biofilm developing on the flat substrate from the eastern wall, near the ground (Fig. 9B).	<i>Muriella terrestris</i>	<i>Chlorella vulgaris</i>	<i>Jenufa minuta</i> HM563744 (99%)
MC2	Thin green biofilm developing on the flat substrate from the left side of the inner arc (Fig. 9C).	<i>Muriella terrestris</i> <i>Symplocastrum friesii</i>	<i>Chlorella vulgaris</i> <i>Ctenocladus circinnatus</i>	<i>Jenufa minuta</i> HM563744 (99%)
MC3	Green biofilm developing on the rough substrate from the ceiling of the tomb (Fig. 9D).	<i>Chroococciopsis</i> sp. <i>Gloeocapsa</i> sp.	<i>Gloeocapsa rupestris</i>	N.D.
MC4	Green biofilm developing on the rough substrate of the left corridor wall of the tomb (Fig. 9E).	<i>Chroococciopsis</i> sp. <i>Gloeocapsa rupestris</i> <i>Symplocastrum friesii</i> <i>Scytonema</i> sp.	<i>Chroococciopsis</i> sp. <i>Gloeocapsa rupestris</i> <i>Symplocastrum friesii</i>	<i>Leptolyngbya</i> sp. HM217061 (99%) <i>Oculatella</i> sp. KC311928 (99%)
MC5	Green biofilm developing on the rough substrate from the northern wall, near the ceiling of the tomb (Fig. 9F).	N.D.	<i>Chroococciopsis</i> sp. <i>Gloeocapsa rupestris</i> <i>Symplocastrum friesii</i>	N.D.

N.D. Not determined

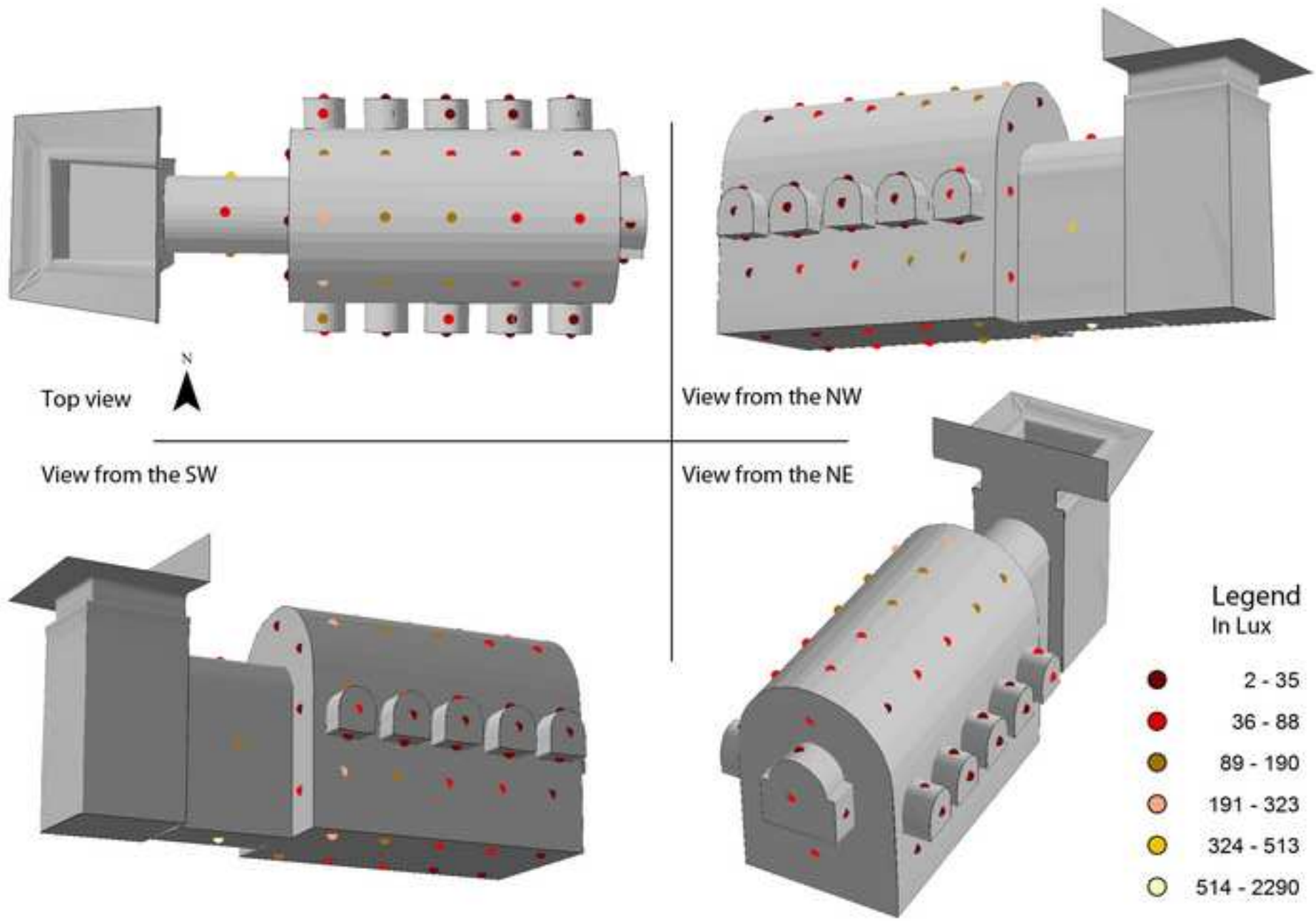
Figure

[Click here to download high resolution image](#)



Figure

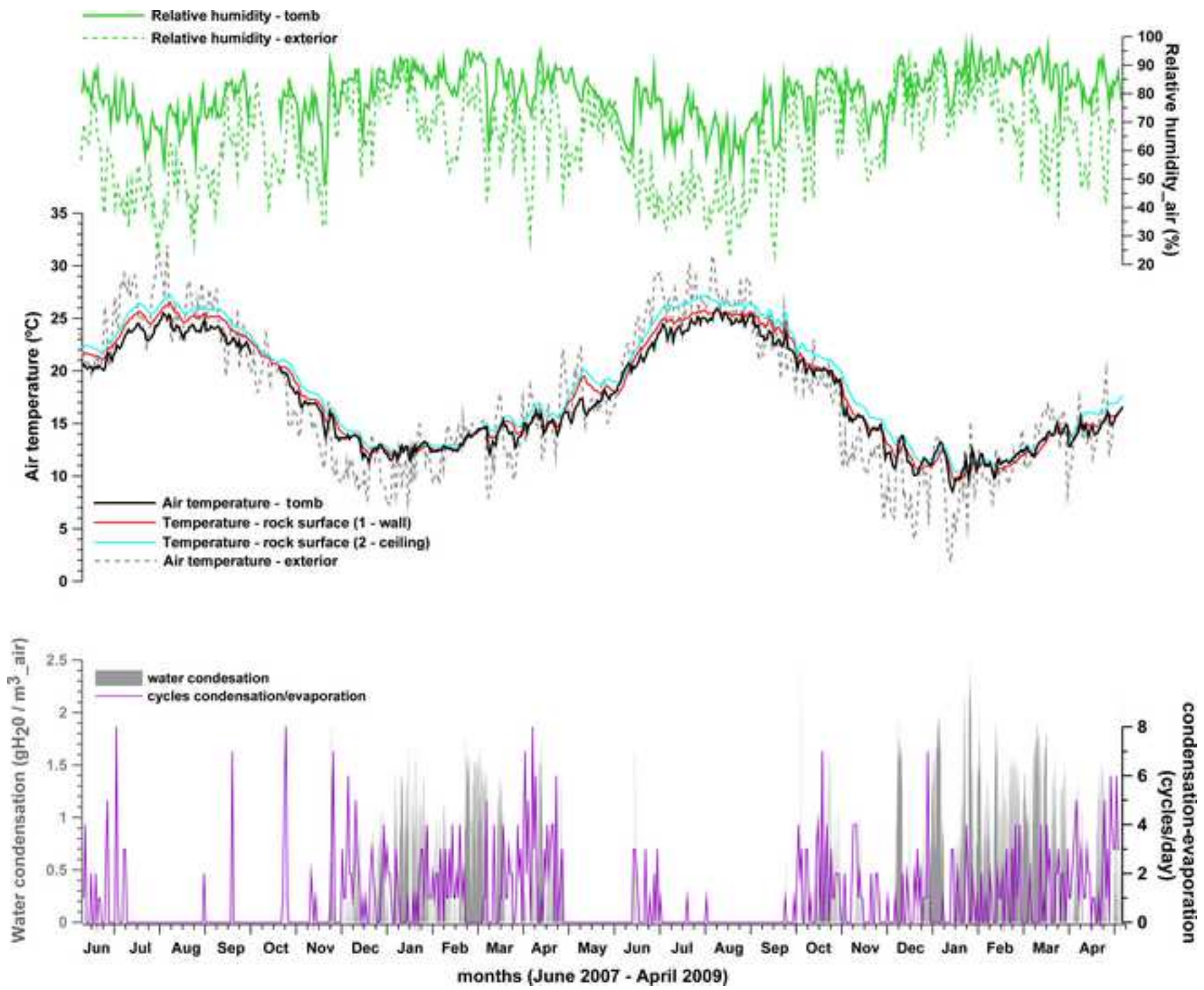
[Click here to download high resolution image](#)





Figure

[Click here to download high resolution image](#)



Figure

[Click here to download high resolution image](#)

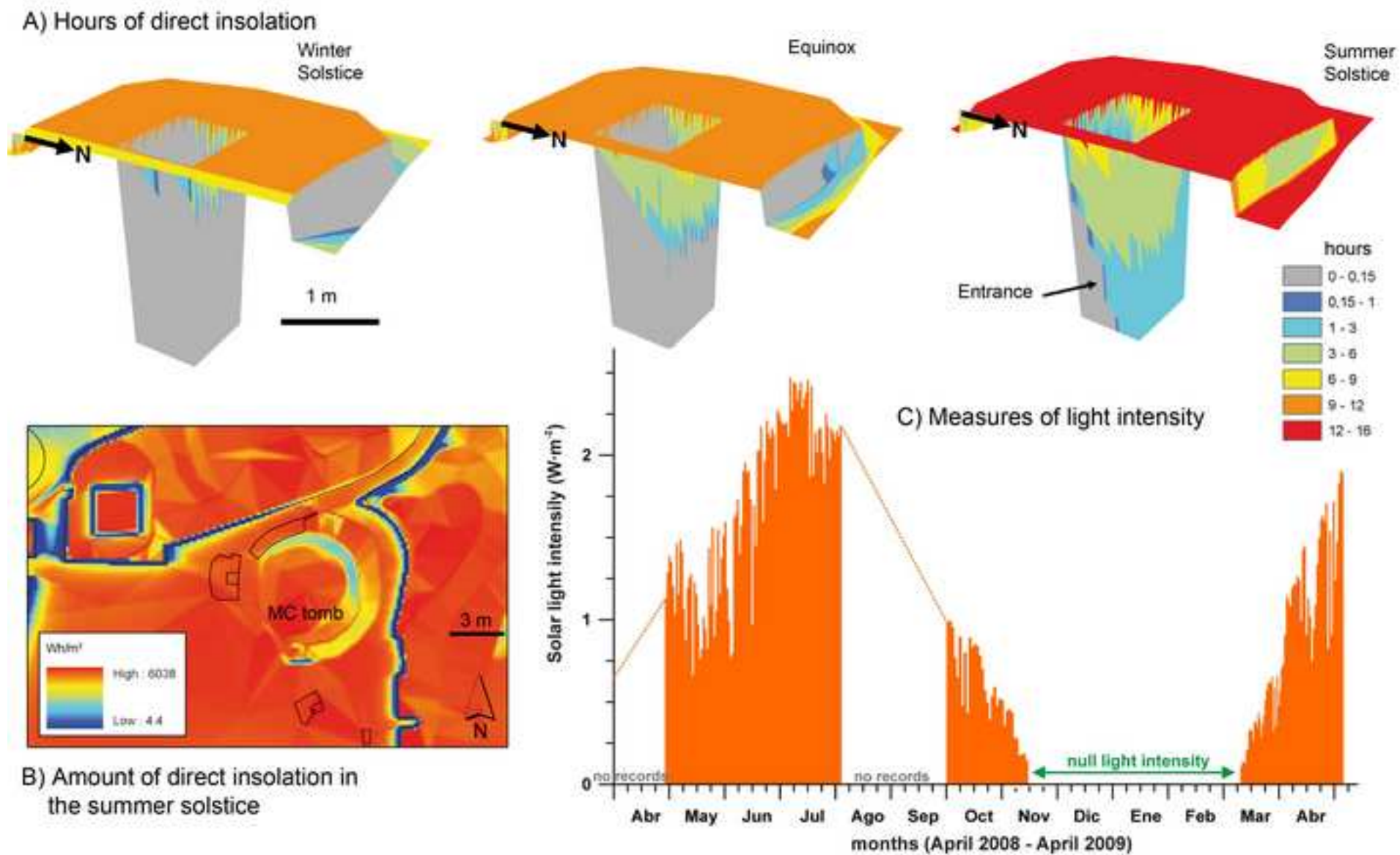
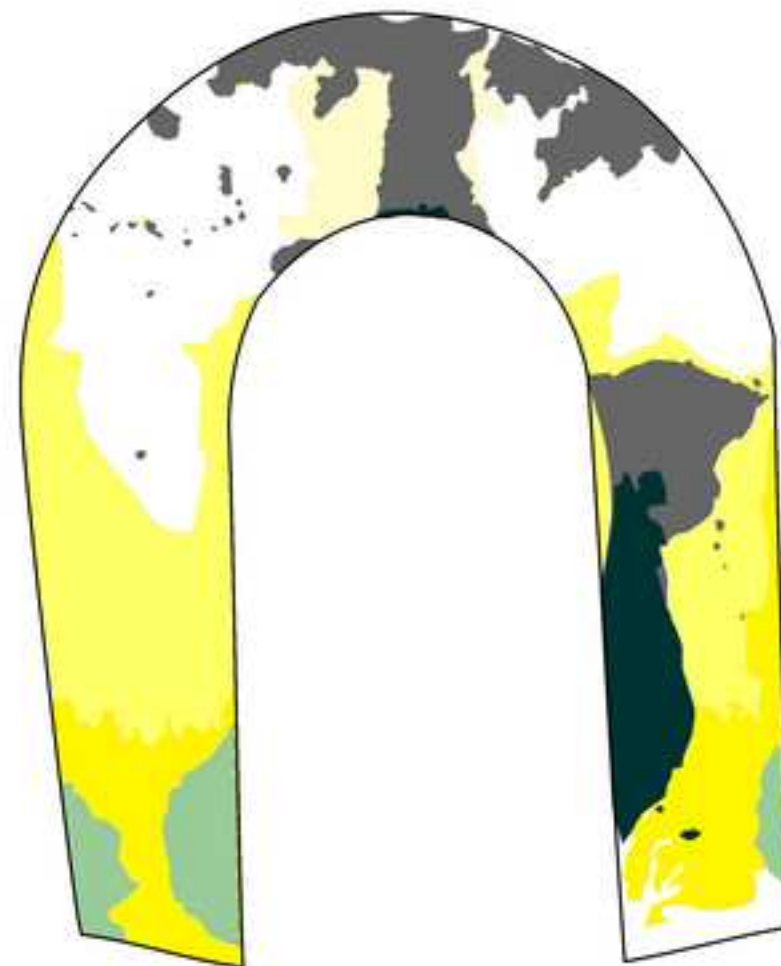





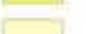


Figure  
[Click here to download high resolution image](#)



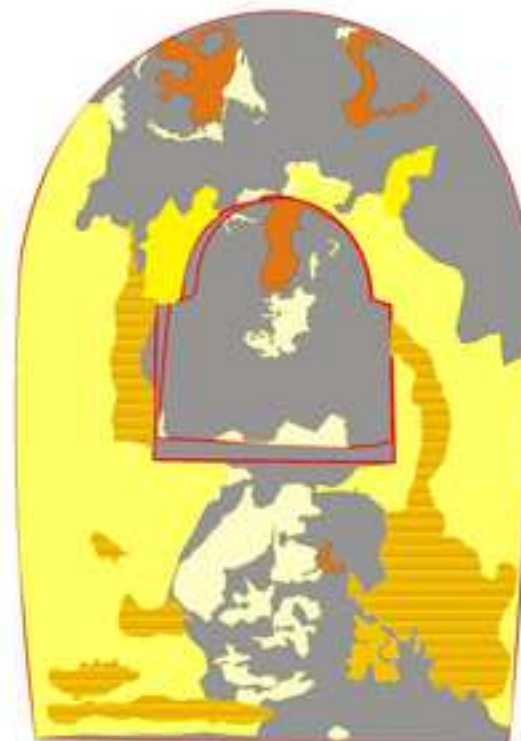
Figure  
[Click here to download high resolution image](#)



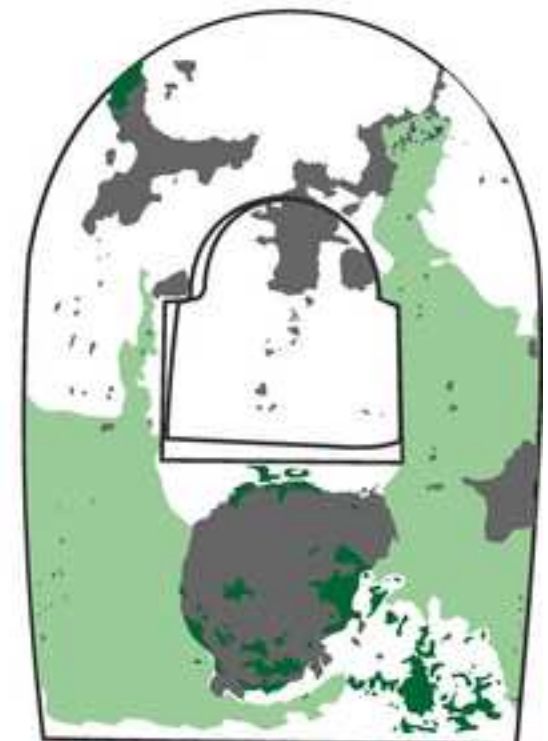
- |  |                             |   |   |
|--|-----------------------------|---|---|
|  | Flaking, scaling, crumbling |  | Continuous smooth coating                                     |
|  | Light green biofilms        |  | Discontinuous smooth coating (disperse gypsum efflorescences) |
|  | Dark green biofilms         |  | Efflorescences  |

Figure

[Click here to download high resolution image](#)

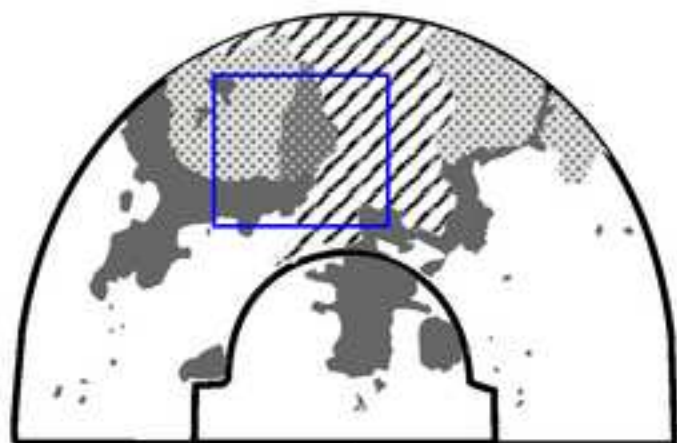
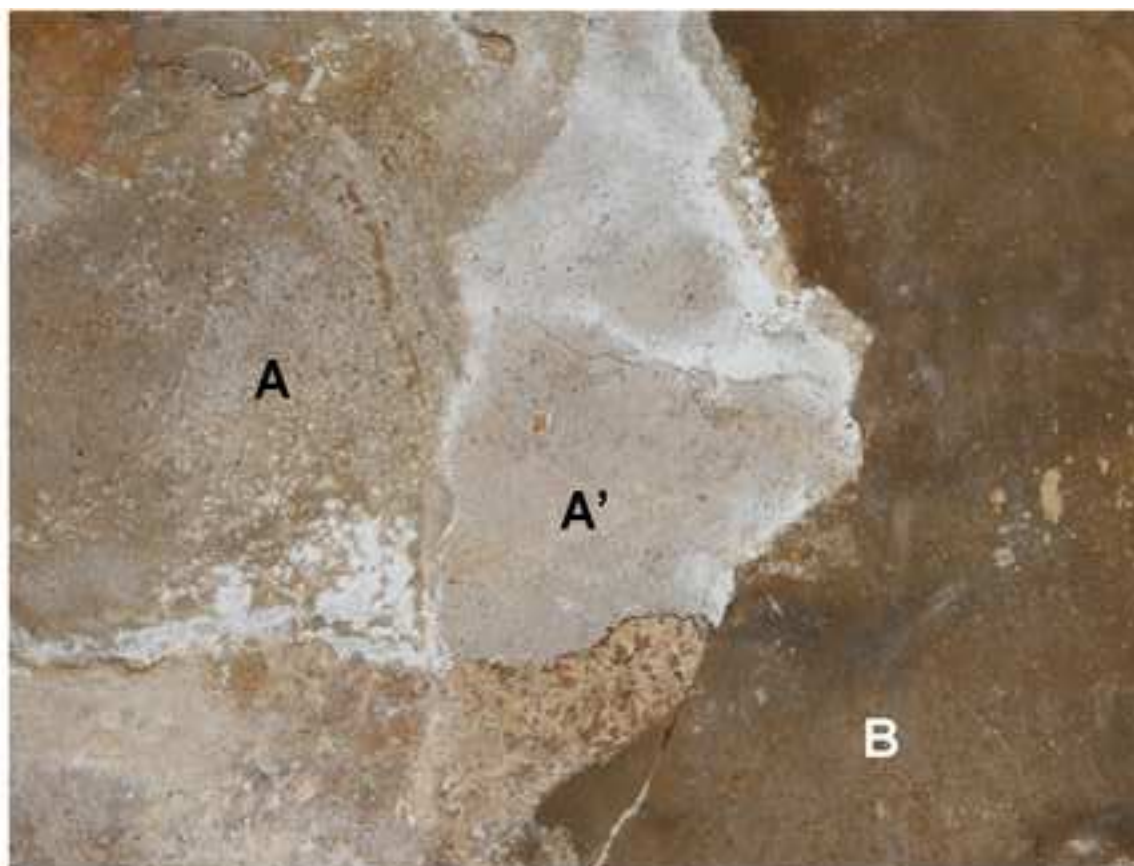


- Orange: Globulitic crust
- Dark orange: Rugose crust
- Yellow: Continuous smooth coating
- Light yellow: Discontinuous smooth coating (gypsum efflorescences)
- White: Undifferentiated efflorescences



- White: Violet colonies
- Light green: Light green biofilms
- Dark green: Dark green biofilms
- Dark grey: Flaking, scaling, crumbling

Figure  
[Click here to download high resolution image](#)




 Restoration materials

Figure  
[Click here to download high resolution image](#)



Figure  
[Click here to download high resolution image](#)

